J Mater Sci (2011) 46:7839–7849
DOI 10.1007/s10853-011-5765-4

Structure and thermodynamics of the key precipitated phases in the Al–Mg–Si alloys from first-principles calculations

Dongdong Zhao · Liangcai Zhou · Yi Kong · Aijun Wang · Jiong Wang · Yingbiao Peng · Yong Du · Yifang Ouyang · Wenqing Zhang

Received: 1 May 2011 / Accepted: 1 July 2011 / Published online: 13 July 2011

Abstract First-principles calculations have been carried out to investigate the structure, stability, and finite-temperature thermodynamic properties of the key precipitates in the Al–Mg–Si alloys including β''-Mg_5Si_6, U1-Al_2MgSi_2, U2-$Al_4Mg_4Si_4$, β'-Mg_9Si_5, and β-Mg_2Si. The calculated phonon densities of states indicate that these precipitated phases are vibrationally stable. Within the framework of the quasiharmonic approach, the finite-temperature thermodynamic properties of these precipitated phases including entropy, enthalpy, and Gibbs free energy have been calculated. The heat capacities at constant pressure for these precipitates are predicted. The finite-temperature entropies of formation, enthalpies of formation, and Gibbs free energy of formation for these precipitates are also computed. The acquired thermodynamic properties are expected to be utilized for the prediction of the metastable equilibria in the Al–Mg–Si alloys.

D. Zhao · L. Zhou · Y. Kong · A. Wang · J. Wang · Y. Peng · Y. Du (✉)
State Key Laboratory of Powder Metallurgy, Central South University, Changsha, Hunan 410083, People's Republic of China
e-mail: yongducalphad@gmail.com

Y. Ouyang
Department of Physics, Guangxi University, Nanning 530004, People's Republic of China

W. Zhang
State Key Laboratory of High Performance Ceramics and Superfine Microstructure, Shanghai Institute of Ceramics, Chinese Academy of Sciences, Shanghai 200050, People's Republic of China

Introduction

The Al–Mg–Si alloys have received considerable attention due to the wide applications of 6xxx alloys in automotive industries [1–7]. These alloys have good extrudability and age hardening characteristics as well as excellent corrosion, surface, and welding properties [5, 8–10], which make them find applications in a wide range of areas, such as in the construction, automobile, and aerospace industries. An increasing demand for the improved control of the properties of the Al–Mg–Si alloys requires knowledge of the finest details of the precipitation sequence, which includes diffusion, solute clustering, nucleation, growth, and transformation of the precipitates. The precipitation sequence of the Al–Mg–Si alloys during age hardening is complex and involves a wide variety of metastable phases (e.g., Guinier–Preston zones (GP-zones), β'', U1, U2, B′, β', β) [5, 9]. The generic precipitation sequence generally accepted for the Al–Mg–Si alloys is as follows [5, 9]:

$$\mathrm{SSSS} \rightarrow \mathrm{GP-zones} \rightarrow \beta''(\mathrm{Mg_5Si_6}) \rightarrow (\mathrm{U1}, \mathrm{U2}, \mathrm{B}', \beta') \rightarrow \beta(\mathrm{Mg_2Si}), \mathrm{Si}$$

where SSSS stands for the supersaturated solid solution, GP-zones are aggregates of solute atoms in the aluminum matrix. Among these metastable precipitate phases, the β'' phase with a monoclinic structure of a composition Mg_5Si_6 [2] is believed to be the most effective strengthening precipitate. Here, the phases U1, U2, and B′ are also referred to "type A", "type B", and "type C" precipitates, respectively [4]. The β' precipitate is in rod shape, and is reported to be present in over-aged specimens [4]. Vissers et al. [11] have determined the detailed structure of β' phase using electron diffraction (ED), and reported that β' has a composition of Mg_9Si_5 [11]. It is worth noting that except for the equilibrium phases β-Mg_2Si and Si, all phases are metastable.

Despite of the importance of this class of alloys, information regarding measurements of the energetics for these metastable precipitate phases is nonexistent in the literature. In addition, quantitative experimental determination of metastable precipitate energetics (e.g., via calorimetry) is often difficult. However, it has recently been demonstrated that first-principles calculations provide a highly valuable and predictive approach for establishing precipitate energetics and studying their transformations. Recently, several groups of authors have investigated the key precipitates in the Al–Mg–Si alloys via first-principles calculations. Frøseth et al. [8] have investigated the bonding and stability of the key precipitates using augmented plane-wave + density-functional theory calculations. Ravi and Wolverton [5] have collected the crystal structures for the key precipitates in the Al–Mg–Si system and investigated the relative stability of the precipitates. Van Huis et al. [9, 10] have performed density functional-based calculations to evaluate the phase stability and structural relations of the matrix-embedded precipitate phases in the Al–Mg–Si alloys in the early and late stages of evolution. Liu et al. [12] have calculated the elastic constants and thermophysical properties of the key precipitates in the Al–Mg–Si alloys via first-principles calculations. It should be noted that a complete set of structural parameters, ground-state, and finite-temperature thermodynamic properties would also provide key inputs to CALPHAD method [13] for the sake of predicting metastable phase equilibria. For example, Zhang et al. [14] have conducted an investigation associated with the solvus boundaries of stable and metastable phases in the Al–Mg–Si system via harmonic approximation and thermodynamic modeling. These considerations motivated us to focus on structure, ground-state, and finite-temperature thermodynamic properties of the key precipitates in the Al–Mg–Si alloys within the approach of quasiharmonic approximation [13, 15].

The rest of this study is organized as follows. In "Theory and methodology", the methodologies for the calculations of structure and finite-temperature thermodynamic properties are presented, and some details on the computation and simulation are introduced. In "Results and discussion", the obtained structures, ground-state, and finite-temperature thermodynamic properties of the precipitated phases in the Al–Mg–Si alloys are discussed, followed by the summary in "Summary".

Theory and methodology

First-principles quasiharmonic approach

The quasiharmonic approach based on first-principles calculations is utilized to calculate the finite-temperature thermodynamic properties of the key precipitates in the Al–Mg–Si alloys. In terms of quasiharmonic approach, the finite-temperature Helmholtz free energy $F_{\mathrm{Hel}}(V,T)$ is represented by [16–18]:

$$F_{\mathrm{Hel}}(V,T) = E(V) + F_{\mathrm{vib}}(V,T) + F_{\mathrm{el}}(V,T). \quad (1)$$

The first term in Helmholtz free energy $E(V)$ is the static energy (without zero-point vibrational energy) at 0 K, which is usually obtained through the fitting of equation of state (EOS). $F_{\mathrm{vib}}(V,T)$and $F_{\mathrm{el}}(V,T)$ are vibrational and thermal electronic contributions to the total free energy, respectively.

In order to calculate the static energy of the precipitated phases in the Al–Mg–Si alloys, the first-principles calculated volume-dependent energy curves are fitted by means of four-parameter Birch–Murnaghan EOS with its linear form given by [18]:

$$E(V) = a + bV^{-2/3} + cV^{-4/3} + dV^{-6/3} \quad (2)$$

where V is volume, and a, b, c, and d are the fitting parameters. The equilibrium properties fitted with EOS include the equilibrium volume (V_0), equilibrium energy (E_0), bulk modulus (B), and its pressure derivative (B'). The lattice vibrational contribution to Helmholtz free energy $F_{\mathrm{vib}}(V,T)$ is described with the well-known harmonic approximation [15] at each fixed volume. With the obtained phonon density of state (DOS), the contribution from lattice vibrations to Helmholtz free energy $F_{\mathrm{vib}}(V,T)$ is often evaluated with [15]:

$$F_{\mathrm{vib}} = k_{\mathrm{B}}T \int_0^{\infty} \ln\left[2\sinh\frac{\hbar\omega}{2k_{\mathrm{B}}T}\right] g(\omega)\mathrm{d}\omega \quad (3)$$

where $\hbar$ and $g(\omega)$ are the reduced Plank constant and the phonon DOS, respectively. The contributions from thermally excited electrons to Helmholtz free energy (F_{el}) can be calculated as:

$$F_{\mathrm{el}} = E_{\mathrm{el}} - \mathrm{TS}_{\mathrm{el}}. \quad (4)$$

The equations for the calculations of E_{el} and S_{el} are described elsewhere [16, 17].

The heat capacity at constant pressure (C_p) is usually described with the following equation [19, 20]:

$$C_p = C_v^{\mathrm{ele}} + C_v^{\mathrm{vib}} + \alpha^2 V_T BT \quad (5)$$

where α is the volume thermal expansion coefficient, and B is the isothermal bulk modulus. V_T is the equilibrium volume at temperature T and pressure P. The heat capacity at constant volume $\left(C_v^{\mathrm{vib}}\right)$ can be calculated via differentiating the free energy of lattice vibrations $F_{\mathrm{vib}}(V,T)$. And C_v^{ele}, which is the thermal electronic contribution to the heat capacity, is described with the following equation:

$$C_v^{\text{ele}} = \frac{1}{k_B}\int n(\varepsilon, V)\exp\left(\frac{\varepsilon-\varepsilon_f}{k_B T}\right)\left(f\cdot\frac{\varepsilon-\varepsilon_f}{T}\right)^2 d\varepsilon \quad (6)$$

where $n(\varepsilon, V)$ is the electronic density of state (eDOS). And ε_f and f are the Fermi energy and Fermi distribution, respectively.

According to Eq. 5, C_p is close to C_v^{vib} at low temperature, larger than C_v^{vib} at high temperature, where the thermal expansion effect of phonons is noticeable. Consequently, the key to calculate C_p from first-principles calculations is to include the main contribution to C_p from the thermal expansion on phonons. The quasiharmonic approximation is accounted for by the harmonic approximation at several volumes in a specific temperature.

In addition, the equilibrium finite-temperature entropies of formation (ΔS_f), enthalpies of formation (ΔH_f), and Gibbs free energy of formation (ΔG_f) for the Al–Mg–Si precipitates are evaluated by the following equation [5]:

$$\Delta E^{\text{eq}}(A_pB_q) = E(A_pB_q) - [x_A E^{\text{eq}}(A) + x_B E^{\text{eq}}(B)] \quad (7)$$

where $E(A_pB_q)$, $E^{\text{eq}}(A)$, and $E^{\text{eq}}(B)$ are the thermodynamic properties (per atom) of the precipitated phases in the Al–Mg–Si alloys A_pB_q and constituents, A and B, each in its equilibrium (zero-pressure) geometry. $x_A = p/(p+q)$ and $x_B = q/(p+q)$ are the concentrations of A and B, respectively. Analogous expressions apply for ternary phases.

Details of first-principles and phonon calculations

The highly efficient first-principles plane-wave pseudopotential method as implemented in the Vienna ab initio simulation package (VASP) [21, 22] is utilized for the present first-principles calculations. The electron–ion interactions are described by the full potential frozen-core PAW method [23, 24], and the exchange–correlation is treated within the Generalized Gradient Approximation (GGA) of Perdew–Burke–Ernzerhof (PBE) [25]. The electronic configurations considered are $3s^23p^1$ for Al, $2p^63s^2$ for Mg, and $3s^23p^2$ for Si, respectively. Convergence tests indicated that a cutoff of 400 eV is sufficient to insure the total energy differences are less than 1 meV/atom. The Monkhorst–Pack scheme [26] k-points sampling together with the linear tetrahedron method including Blöchl corrections [27] is adopted for the integration in the Brillouin zone (BZ). The convergence criterion for electronic self-consistency and ionic relaxation loop are 10^{-6} eV and 10^{-3} eV/Å, respectively. In the present calculations, the unit cells of the key precipitates in the Al–Mg–Si alloys are fully relaxed with respect to the volume, the shape of the unit cell, and the atomic positions.

The phonon calculations are performed within the frozen phonon (supercell method) approach as implemented in the ATAT package [28], with VASP as the computational engine. In the quasiharmonic approach, five volumes are generated for each key precipitated phase in the Al–Mg–Si alloys. The displacement of 0.05 Å around the equilibrium positions of each atom in the supercell is applied, and the calculated forces acting on each atom are then fitted to obtain the force constants. The cutoff distance of 6 Å is adopted to fit the force constants and to obtain the phonon frequencies in this study. The total number of k-points per reciprocal atom is at least 10000 for all the supercells. Additional details of phonon methodology can be found elsewhere [29].

The mixed-space approach to first-principles calculations of phonon frequencies as implemented in the Yphon package [30] is utilized to predict Longitudinal Optical/Transverse Optical (LO/TO) splitting in β-Mg_2Si. This approach can make full use of the accuracy of the force constants calculated in real space and the dipole–dipole interactions in reciprocal space [30]. In calculating the Born effective charge tensor and the high frequency static dielectric tensor, we employed the linear response theory implemented in VASP 5.2 by Gajdoš et al. [31] and the same parameter settings as the static calculations. To calculate the force constants in real space, we used the energy cutoff of 400 eV, together with $2 \times 2 \times 2$ supercells (of the conventional cell) and $6 \times 6 \times 6$ k-mesh sampling for β-Mg_2Si.

Results and discussion

In this section, first we show the crystal structures and equilibrium properties of the pure elements and Al–Mg–Si key precipitates predicted by EOS fittings (Sect. Crystal structures), and then the thermodynamic properties of pure elements at finite temperatures predicted by Eq. 1 and compared with the results from Scientific Group Thermodata Europe (SGTE) data [32] (Sect. Finite-temperature thermodynamic properties of pure elements). To demonstrate the reliability of the present calculations, the phonon and heat capacity of β-Mg_2Si in comparison with the results from experiments, CALPHAD modeling and previously theoretical results are presented (Sect. Phonon and heat capacity of β-Mg_2Si). Section Finite-temperature thermodynamic properties and stability of the key precipitates) shows the finite-temperature thermodynamic properties of the Al–Mg–Si key precipitates.

Crystal structures

The presently calculated structural information of pure elements (Al, Mg, and Si) and the key precipitates in the Al–Mg–Si alloys are summarized in Table 2, compared

with available experimental data. It should be noted that the equilibrium states of the elements are taken as the reference states. The comparisons shown in Table 1 reveal that the results from first-principles calculations agree reasonably well with the experimental data [33–35]. The discrepancies for the key precipitates are due to the fact that the lattice constants from first-principles are in a stress-free situation while the precipitated phases are strained by Al-matrix. The structures of these precipitated phases are considerably influenced by the interfacial and strain energies [5].

The volume–dependent energy curves of the key precipitates in the Al–Mg–Si alloys are fitted through Eq. 2. Figure 1a–c shows the volume–dependent energy curves and the fitted EOS's of these precipitated phases, indicating that the EOS's fit well with the VASP calculated energies. Through EOS fittings, the bulk modulus and its pressure derivative of individual precipitated phase in the Al–Mg–Si alloys are obtained and shown in Table 1, in comparison with the available experimental and theoretical results [12, 36–41]. As can be seen in Table 1, the presently determined bulk modulus of the precipitates is in good agreement with the results from [12, 36]. While for the elements Al, Mg, and Si, the agreement is reasonably good except for Si. The calculated bulk modulus of Si is about underestimated by 9.7% compared with the experimental value [38]. In addition, the pressure derivative of the bulk modulus for the elements and precipitates coincide well with the experimental and theoretical results.

Finite-temperature thermodynamic properties of pure elements

By considering both the vibrational and thermal electronic contributions, the predicted thermodynamic properties (Gibbs energy G, entropy S, enthalpy H, and heat capacity C_p at zero external pressure) of fcc-Al, hcp-Mg, and diamond-Si are predicted and shown in Figs. 2, 3, and 4, together with the SGTE data [32] estimated in terms of experiments for comparison. The reference states of fcc-Al, hcp-Mg, and diamond-Si are the commonly used ones in

Table 1 Crystal structures and bulk modulus for the key precipitates in the Al–Mg–Si system

Phase	Structure	Pearson symbol	Space group	Lattice parameter (Å)						$^{a}B_0$ (GPa)	$^{a}B_0'$	Ref.
				GGA-PBE			Expt.					
				a	*b*	*c*	*a*	*b*	*c*			
Al	Cub.	*cF4*	Fm-3 m	4.04	–	–	4.05	–	–	[a]77.30	[a]4.83	[34]
										[b]79.40	[g]4.69	
Mg	Hex.	*hP2*	$P6_3/mmc$	3.18	–	5.20	3.21	–	5.21	[a]36.53	[a]4.14	[33]
										[c]35.83	[g]4.12	
Si	Cub.	*cF8*	Fd-3 m	5.46	–	–	5.43	–	–	[a]89.17	[a]4.34	[35]
										[d]98.80	[h]4.24	
β''-Mg_5Si_6	Mon.	*mS22*	C2/m	15.14	4.05	6.94 ($\beta = 110^\circ$)	15.13	4.05	6.74 ($\beta = 105^\circ$)	[a]61.90	[a]4.62	[2]
										[e]67.00	–	
U1-Al_2MgSi_2	Tri.	*hP5*	P-3m1	4.08	–	6.66	4.05	–	6.74	[a]61.41	[a]4.37	[7]
										[f]61.59	[f]4.42	
U2-$Al_4Mg_4Si_4$	Ort.	*oP12*	Pnma	6.59	4.05	8.03	6.75	4.05	7.94	[a]66.48	[a]4.54	[6]
										[h]65.69	[f]4.47	
β'-Mg_9Si_5	Hex.	*hP14*	$P6_3/m$	7.16	–	12.29	7.15	–	12.15	[a]59.95	[a]4.13	[11]
										[f]58.69	[f]4.51	
β-Mg_2Si (stable)	Cub.	*cF12*	Fm-3 m	6.36	–	–	6.34	–	–	[a]54.73	[a]4.09	[57]
										[f]54.60	[f]4.08	

The data for elements are also collected in the table

[a] Evaluated from EOS fitting in this study

[b] Ref [37], experiment

[c] Ref [39], experiment

[d] Ref [38], experiment

[e] Ref [36], theoretically predicted

[f] Ref [12], theoretically predicted

[g] Ref [41], theoretically predicted

[h] Ref [40], experiment

CALPHAD community, i.e., the enthalpy at 298.15 K and 1 bar. As can be seen in Fig. 2, the present prediction of thermodynamic properties for fcc-Al is in good agreement with the SGTE data. As for hcp-Mg, the presently predicted thermodynamic properties including G, S, and H are in good coincidence with the SGTE data. As shown in Fig. 3, the calculated C_p of hcp-Mg is also in good agreement with the SGTE values at lower temperatures; however, the discrepancies become larger as the temperature increases. For diamond-Si, the calculated thermodynamic properties including G, S, and H in this study are in good coincidence with the SGTE data. The evaluated C_p of diamond-Si coincides with the SGTE data at lower temperatures, showing some deviations with SGTE values in a high-temperature range. It should be emphasized that the SGTE data at lower temperatures (below 300 K) are not shown for comparison due to the inaccuracy of SGTE data at lower temperatures [32]. In general, the presently calculated thermodynamic properties including G, S, H, and C_p at zero external pressure of fcc-Al, hcp-Mg, and diamond-Si are in good agreement with the SGTE data, which are the representative of the experimental data.

Phonon and heat capacity of β-Mg_2Si

β-Mg_2Si is known to be a small band gap semiconductor [42, 43]. In a consequence, the Coulomb interactions will cause the frequencies of LO modes to be above those of TO modes. The LO/TO splitting occurs at the Γ point of the BZ, and only for infrared active modes. However, the traditional frozen phonon approach cannot be employed to estimate the LO/TO splitting directly. Zhang et al. [14] has utilized frozen phonon approach to calculate the phonon dispersions for β-Mg_2Si without predicting the LO/TO splitting for the infrared active mode. In this study, the mixed-space approach [30] and frozen phonon approach are both utilized to calculate the phonon dispersions of β-Mg_2Si. It is worth noting that only the ancillary calculations concerned with LO/TO splitting are performed for β-Mg_2Si, where the experimental data are available. Figure 5 shows the calculated phonon dispersions for β-Mg_2Si using mixed-space approach and frozen phonon method in comparison with the experimental data. As shown in Fig. 5a, the calculated phonon dispersions at Γ point (including LO and TO) for β-Mg_2Si using mixed-space

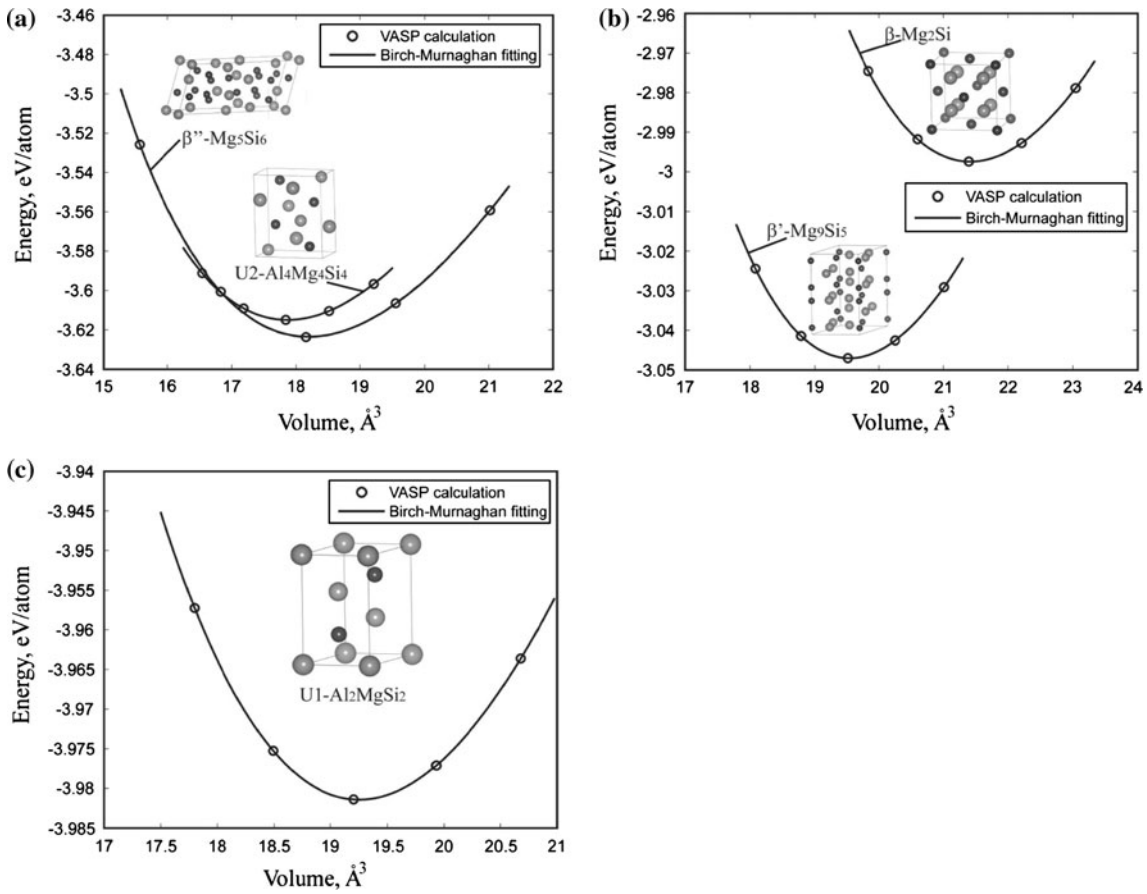

Fig. 1 Calculated energy versus volume points (*open circles*) for β''-Mg_5Si_6, U1-Al_2MgSi_2, U2-$Al_4Mg_4Si_4$, β'-Mg_9Si_5, β-Mg_2Si, and the correspondingly fitted four-parameter Birch–Murnaghan equation of states (*Solid lines*)

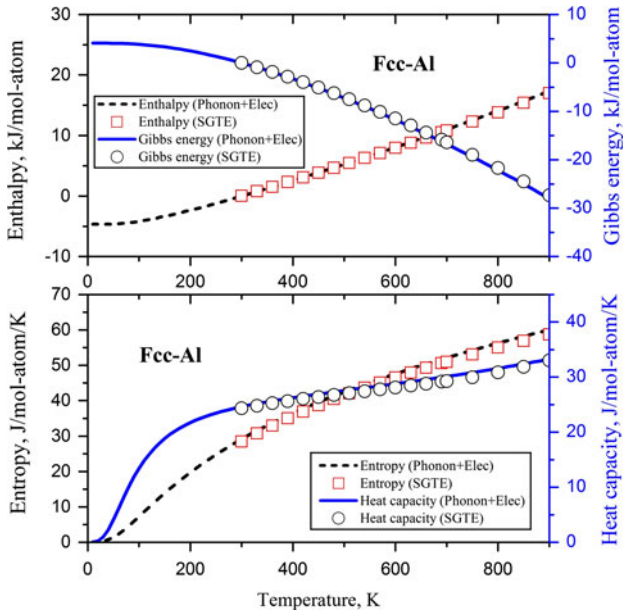

Fig. 2 Predicted thermodynamic properties (Gibbs energy G, enthalpy H, entropy S, and heat capacity C_p) of fcc-Al by considering both the vibrational and thermal electronic contributions. The reference state for H is the value at 298.15 K. The SGTE data are also shown for comparison

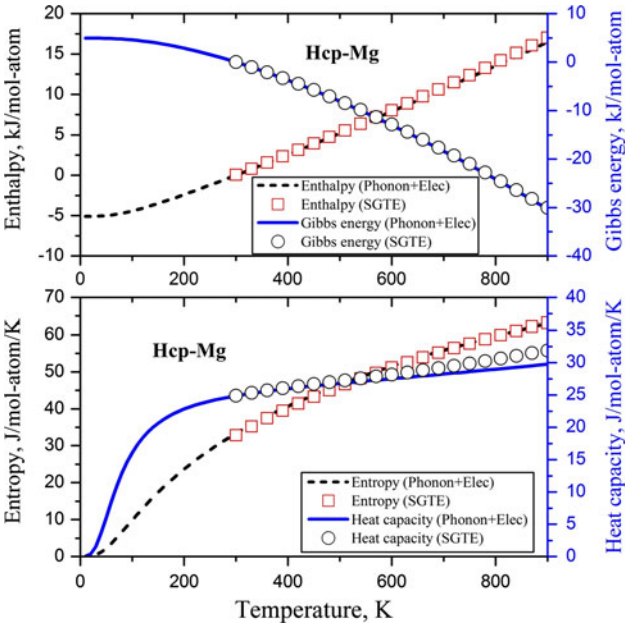

Fig. 3 Predicted thermodynamic properties (Gibbs energy G, enthalpy H, entropy S, and heat capacity C_p) of hcp-Mg by considering both the vibrational and thermal electronic contributions. The reference state for H is the value at 298.15 K. The SGTE data are also shown for comparison

approach are in good agreement with the experimental values [44, 45]. While the frozen phonon approach cannot correctly predict the LO phonon frequency, as shown in

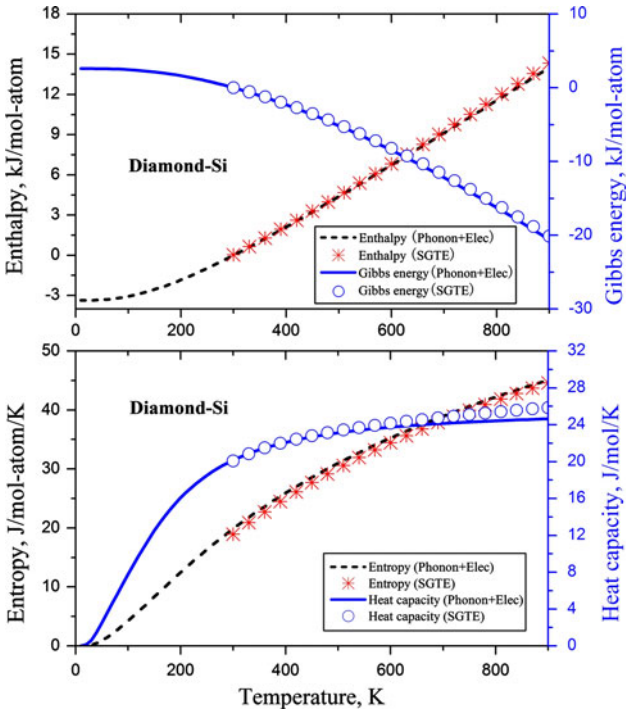

Fig. 4 Predicted thermodynamic properties (Gibbs energy G, enthalpy H, entropy S, and heat capacity C_p) of diamond-Si by considering both the vibrational and thermal electronic contributions. The reference state for H is the value at 298.15 K. The SGTE data are also shown for comparison

Fig. 5b. Table 2 collects the phonon frequencies at high-symmetry points in the first BZ for β-Mg_2Si. Using the mixed approach, the phonon frequencies for LO/TO branches at Γ point are in good agreement with the experimental results as shown in Table 2. The frozen phonon predicted that phonon frequency of LO branch is the same with TO at Γ point, thus this phenomenon is inaccurate. Such a feature indicates the inability of frozen phonon approach in predicting LO/TO splitting. It should be noted that the presently determined phonon frequencies at high-symmetry points (Γ, X, W) using the mixed-space approach are very close to the result by Tani [42], who has utilized Density Functional Perturbation Theory (DFPT) [46] to calculate the phonon properties of β-Mg_2Si.

Based on the phonon density of states (DOS) of β-Mg_2Si calculated by means of ATAT package [28], the thermodynamic properties of β-Mg_2Si including entropy, enthalpy, Gibbs free energy, and heat capacity are evaluated by considering both the vibrational and thermal electronic contributions. It also should be mentioned that the LO modes contribute very little to the phonon DOS. Therefore, this study does not take into account the influence of LO/TO splitting on the thermodynamic properties of β-Mg_2Si. Figure 6 shows the calculated heat capacity at constant pressure C_p and heat capacity at constant volume

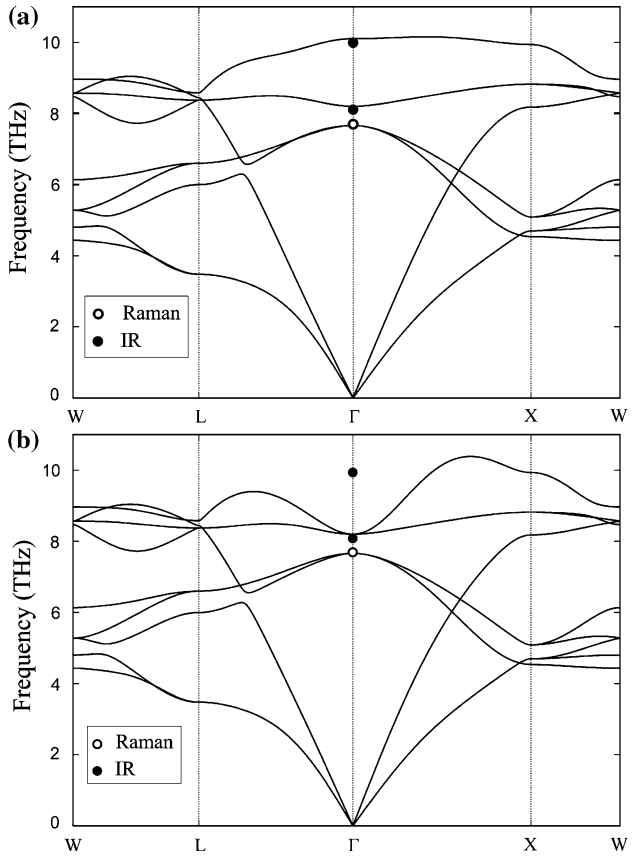

Fig. 5 Calculated phonon dispersions for β-Mg_2Si using mixed approach (**a**) and frozen phonon method (**b**) in comparison with the experimental data

Table 2 Phonon frequencies at high-symmetry points in the first Brillouin zone for β-Mg_2Si

Method	Expt.	Literature		This study	
		Wang et al. [43]	Tani and Kido [42]	Mixed approach	Frozen phonon
$\omega_{TO}(\Gamma)$ (THz)	[a]8.0	8.67	8.2	8.17	8.18
$\omega_{LO}(\Gamma)$ (THz)	[a]9.8	10.43	10.1	10.11	8.18
$\omega_{LA}(X)$ (THz)	–	8.37	8.2	8.18	8.18
$\omega_{TA}(X)$ (THz)	–	4.97	4.7	4.71	4.70
$\omega_{LA}(L)$ (THz)	–	8.42	8.5	8.52	8.51
$\omega_{TA}(L)$ (THz)	–	3.56	3.4	3.47	3.47

[a] From Ref. [44]

C_v of β-Mg_2Si in comparison with the experimental [47], CALPHAD [48] and previously calculated data [43]. As shown in Fig. 6, the presently determined C_p of β-Mg_2Si is in good agreement with the experimental value which is mainly distributed at lower temperatures. The CALPHAD evaluated C_p of β-Mg_2Si bears deviations from the presently calculated results in mid-temperature range from about 300 to 700 K. It is worth noting that the presently determined C_v of β-Mg_2Si is in good coincidence with the previously calculated results by Wang [43]. These comparisons validate the accuracy of the present predictions.

Finite-temperature thermodynamic properties and stability of the key precipitates

Figure 7 illustrates the predicted phonon DOS's for the key precipitates β''-Mg_5Si_6, U1-Al_2MgSi_2, U2-$Al_4Mg_4Si_4$, β'-Mg_9Si_5, and β-Mg_2Si at their theoretical equilibrium volumes. These phonon DOS's can be used to calculate the vibrational contributions to Helmholtz free energy (or Gibbs free energy due to the zero external pressure used in this study). It should be noted that these phonon DOS's are calculated by means of ATAT code [28]. No existence of any imaginary frequency in the phonon DOS's indicates the vibrational stability of the energetically metastable precipitates.

Based on the obtained phonon DOS's and electronic DOS's, the Helmholtz free energy $F_{\mathrm{Hel}}(V,T)$ of the Al–Mg–Si key precipitates can be evaluated according to Eq. 1. Figure 8a–b shows the calculated Gibbs free energies (a) and entropies (b) for the key precipitates in the Al–Mg–Si alloys by considering both the vibrational contributions and thermal electronic contributions. As can be seen in Fig. 8a, $F_{\mathrm{Hel}}(V,T)$ is larger than 0 at 0 K since there exists zero-point energy from lattice vibrations. Comparing the phonon DOS's of the Al–Mg–Si key precipitates as shown in Fig. 5, the distributions of vibrational frequencies in the lower frequency region increase from β-Mg_2Si, U1-Al_2MgSi_2, β'-Mg_9Si_5, U2-$Al_4Mg_4Si_4$ to β''-Mg_5Si_6, indicating the increase of phonon contributions to Gibbs energies from β-Mg_2Si, U1-Al_2MgSi_2, β'-Mg_9Si_5, U2-$Al_4Mg_4Si_4$ to β''-Mg_5Si_6 (cf. Eq. 3 and Fig. 8). In principle, the higher value of the phonon density of states in the lower frequency region implies a weak bonding nature in the precipitates. That is why that the entropy of β''-Mg_5Si_6 increases with temperature more quickly than those of the other key Al–Mg–Si precipitated phases. And consequently, the Gibbs free energy of β''-Mg_5Si_6 decreases faster than that of any other precipitate at high temperatures.

The heat capacities at constant pressure C_p for the key precipitated phases in the Al–Mg–Si alloys are predicted based on Eq. 5 and are plotted as a function of temperature in Fig. 9. It should be noted that there are no experimental data concerned with the C_p of the key precipitated phases in the Al–Mg–Si alloys in the literature up to now except for β-Mg_2Si, which has been discussed above. The C_p is very important in evaluating phase equilibrium via thermodynamic modeling. Since there are no experimental data concerned with the C_p of the key precipitated phases in the Al–Mg–Si alloys, the presently determined C_p of the key precipitated phases are expected to be used to establish the

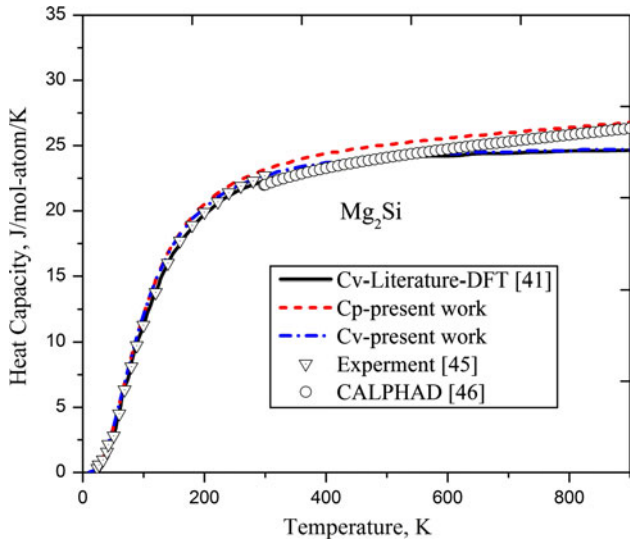

Fig. 6 Calculated heat capacity at constant pressure C_p and heat capacity at constant volume C_v of Mg_2Si in comparison with the experimental, CALPHAD, and previous first-principles calculated data

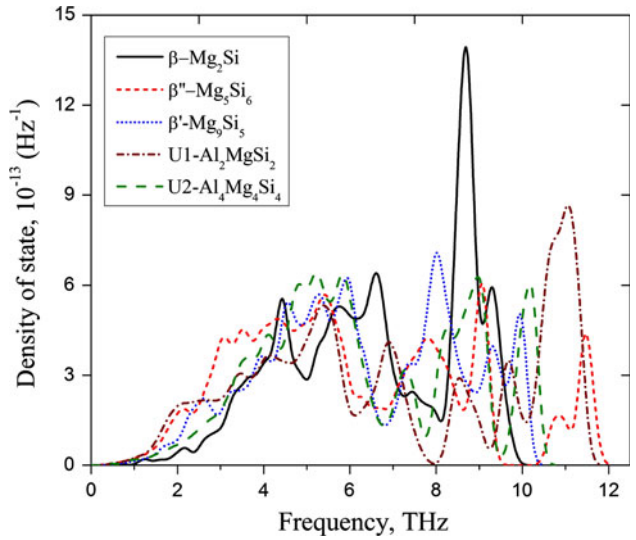

Fig. 7 Calculated phonon density of states (DOS's) for β''-Mg_5Si_6, U1-Al_2MgSi_2, U2-$Al_4Mg_4Si_4$, β'-Mg_9Si_5, and β-Mg_2Si at their theoretical equilibrium volumes

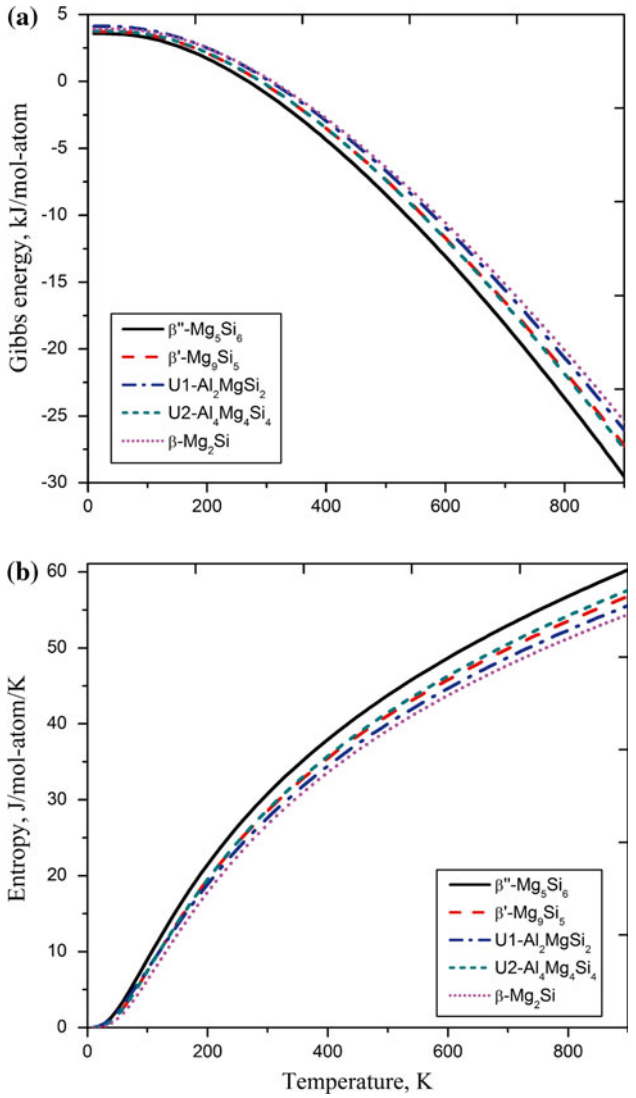

Fig. 8 Calculated Gibbs free energies (**a**) and entropies (**b**) for the key precipitates β''-Mg_5Si_6, U1-Al_2MgSi_2, U2-$Al_4Mg_4Si_4$, β'-Mg_9Si_5, and β-Mg_2Si of the Al–Mg–Si alloys by considering both the vibrational by phonon and thermal electronic contributions based on quasi-harmonic approach. The reference states are fcc-Al, hcp-Mg, and diamond-Si

database of metastable equilibria in the Al–Mg–Si alloys. Figure 10 shows the calculated ΔS_f for the key precipitated phases. The magnitude of this formation property is generally small, with most entropies being slightly positive or negative except for β''-Mg_5Si_6, the ΔS_f of which gradually gets large with the increase of temperature. It can be seen in Fig. 10 that the ΔS_f calculated at a specific temperature decrease in an order like the following sequence: $\Delta S_f(\beta''\text{-}Mg_5Si_6) > \Delta S_f(\text{U2-}Al_4Mg_4Si_4) \approx \Delta S_f(\text{U1-}Al_2MgSi_2)$ $> \Delta S_f(\beta'\text{-}Mg_9Si_5) > \Delta S_f(\beta\text{-}Mg_2Si)$. The metastable phase β''-Mg_5Si_6 has the highest ΔS_f, while the stable phase β-Mg_2Si has the lowest ΔS_f.

Table 3 collects the predicted room temperature (298 K) ΔS_f and ΔH_f of the key precipitated phases in the Al–Mg–Si alloys in comparison with the values obtained from different methods including experiment [47, 49–56], CALPHAD [48], and previous first-principles calculations [5, 14]. It should be noted that these quantities are calculated from a combination of the total energy at 0 K, thermodynamic phonon, and thermal electronic contributions. The ΔH_f calculated at 298 K decrease in an order like:

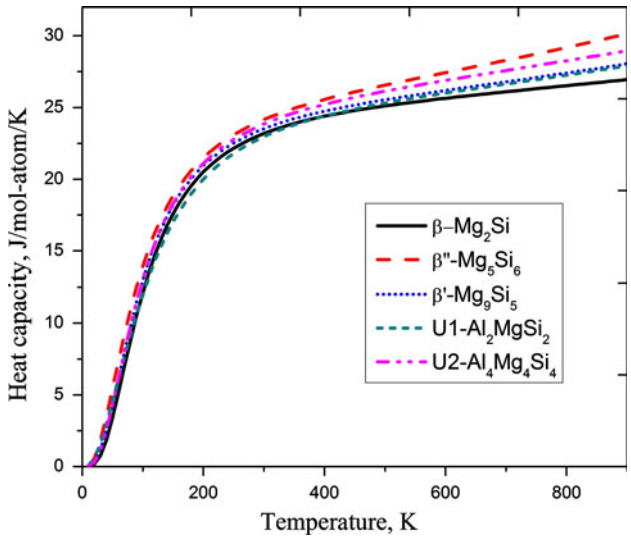

Fig. 9 Calculated heat capacity at constant pressure by considering both the vibrational by phonon and thermal electronic contributions based on quasiharmonic approach for the key precipitates β''-Mg_5Si_6, U1-Al_2MgSi_2, U2-$Al_4Mg_4Si_4$, β'-Mg_9Si_5, and β-Mg_2Si of the Al–Mg–Si alloys

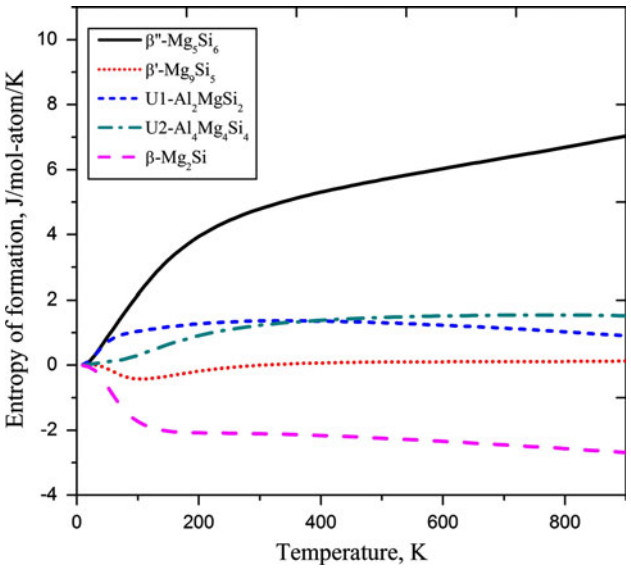

Fig. 10 Calculated entropies of formation versus temperature based on quasiharmonic approach for the key precipitates β''-Mg_5Si_6, U1-Al_2MgSi_2, U2-$Al_4Mg_4Si_4$, β'-Mg_9Si_5, and β-Mg_2Si of the Al–Mg–Si alloys

Table 3 Enthalpies and entropies of formation ΔH_f (kJ/mol-atom) and ΔS_f (J/mol-atom/K) at 298.15 K for the key precipitates β''-Mg_5Si_6, U1-Al_2MgSi_2, U2-$Al_4Mg_4Si_4$, β'-Mg_9Si_5, and β-Mg_2Si of the Al–Mg–Si alloys

Phase	ΔH_f	ΔS_f	Method	Reference
β''-Mg_5Si_6	3.312	4.795	This study	–
	3.5	4.5	First-principles	Zhang et al. [14]
	3.3	–	First-principles	Ravi and Wolverton [5]
U1-Al_2MgSi_2	−0.7530	1.362	This study	–
	−3.1	–	First-principles	Ravi and Wolverton [5]
U2-$Al_4Mg_4Si_4$	−4.506	1.228	This study	–
	−5.8	–	First-principles	Ravi and Wolverton [5]
β'-Mg_9Si_5	−11.552	−0.001	This study	–
	−12.6	0.2	First-principles	Zhang et al. [14]
	−11.7	–	First-principles	Ravi and Wolverton [5]
β-Mg_2Si	−15.677	−2.107	This study	–
	−17.7	−1.8	First-principles	Zhang et al. [14]
	−18.0	–	First-principles	Ravi and Wolverton [5]
	−25.9	–	Calorimetry	Kubaschewski and Villa [49]
	−14.2	3.1	VPTM	Grjotheim et al. [50]
	−27.9	–	Knudsen cell	Ryabchikov and Mikulinski [51]
	−26.4	−7.3	emf	Lukashenko and Eremenko [52]
	–	−0.5	Calorimetry	Mannchen and Jacobo [53]
	−61.9	–	Knudsen cell	Caulfield and Hudson [54]
	−27.1	−2.7	Calorimetry	Gerstein et al. [47]
	−29.7	–	Calorimetry	Blachnik et al. [55]
	−22.2	−4.7	emf	Rao et al. [56]
	−21.1	–	Calorimetry	Feufel et al. [58]
	−21.0	−1.7	CALPHAD	Yuan et al. [48]

VPTM vapor pressure transformation method

emf electromotive force

$\Delta H_f(\beta''\text{-}Mg_5Si_6) > \Delta H_f(\text{U1-}Al_2MgSi_2) > \Delta H_f(\text{U2-}Al_4Mg_4Si_4) > \Delta H_f(\beta'\text{-}Mg_9Si_5) > \Delta H_f(\beta\text{-}Mg_2Si)$. In this order, the β''-Mg_5Si_6 phase, the ΔH_f of which is slightly positive, forms early in the precipitation sequence and gradually disappears after further heat treatment. The phenomenon that the phases U1-Al_2MgSi_2 and U2-$Al_4Mg_4Si_4$ have

lower ΔH_f than β''-Mg_5Si_6 can be accounted for by the fact that the Al atoms have more covalent nature in these Al-containing phases. And this nature has been verified by Frøseth et al. [8], using augmented plane-wave + density-functional theory calculations. With higher Mg content, the β'-Mg_9Si_5 phase bears a lower ΔH_f than the above three phases. The β-Mg_2Si phase which has the final equilibrium structure of the precipitation sequence has the lowest ΔH_f. It should be noted that the first-principles calculated results show a correlation between decreasing energy and increasing Mg:Si ratio as the precipitation process proceeds (except for U1-Al_2MgSi_2 which has the lowest Mg:Si ratio). This result is consistent with the previous first-principles calculations by Ravi and Wolverton [5]. As can be seen in Table 3, the presently determined ΔH_f of the key precipitated phases in the Al–Mg–Si alloys are generally in good agreement with the experimental, CALPHAD, and previous first-principles calculated results. The presently predicted entropies of formation ΔS_f of the key precipitated phases in the Al–Mg–Si alloys in this study are in good agreement with the determined values from Zhang et al. [14] who has utilized harmonic approximation to investigate the thermodynamic properties of the precipitates. The calculated ΔS_f of β-Mg_2Si at 298.15 K yields a value of −2.107 J/mol-atom/K which falls in the range of the experimental data [47, 50, 52, 53, 56] from −7.3 to 3.1 J/mol-atom/K as shown in Table 3.

Figure 11a, b shows the calculated ΔH_f (a) and ΔG_f (b) versus temperature based on quasiharmonic approach for the key precipitates in the Al–Mg–Si alloys, where both the contributions from lattice vibrations and thermally excited electrons to the free energy are considered. From Fig. 11a, it can be concluded that the ΔH_f of these precipitates are almost constant in the studied temperature range, which confirms the reliability of the method for the usual constant treatment of the enthalpy of formation in the thermodynamic optimization, as used in CALPHAD method. As can be seen in Fig. 11b, the ΔS_f has a considerable influence on the ΔG_f of these precipitates, especially for β''-Mg_5Si_6 which has the highest ΔS_f among the precipitates. However, the contribution of ΔS_f to the ΔG_f of these precipitates generally does not convert the relative stability of the precipitates. It can be seen in Fig. 11b that the decrease order of the ΔG_f of these precipitates at a specific temperature (below 800 K) is $\Delta G_f(\beta''\text{-}Mg_5Si_6) > \Delta G_f(\text{U1-}Al_2MgSi_2) > \Delta G_f(\text{U2-}Al_4Mg_4Si_4) > \Delta G_f(\beta'\text{-}Mg_9Si_5) > \Delta G_f(\beta\text{-}Mg_2Si)$, which is the same with the sequence of ΔH_f at a specific temperature for the key precipitates. The key reason for this phenomenon is that the ΔS_f of these precipitates are slightly positive or negative, making the temperature effect upon the change of relative stability of the precipitates at finite-temperatures relatively small (except β''-Mg_5Si_6).

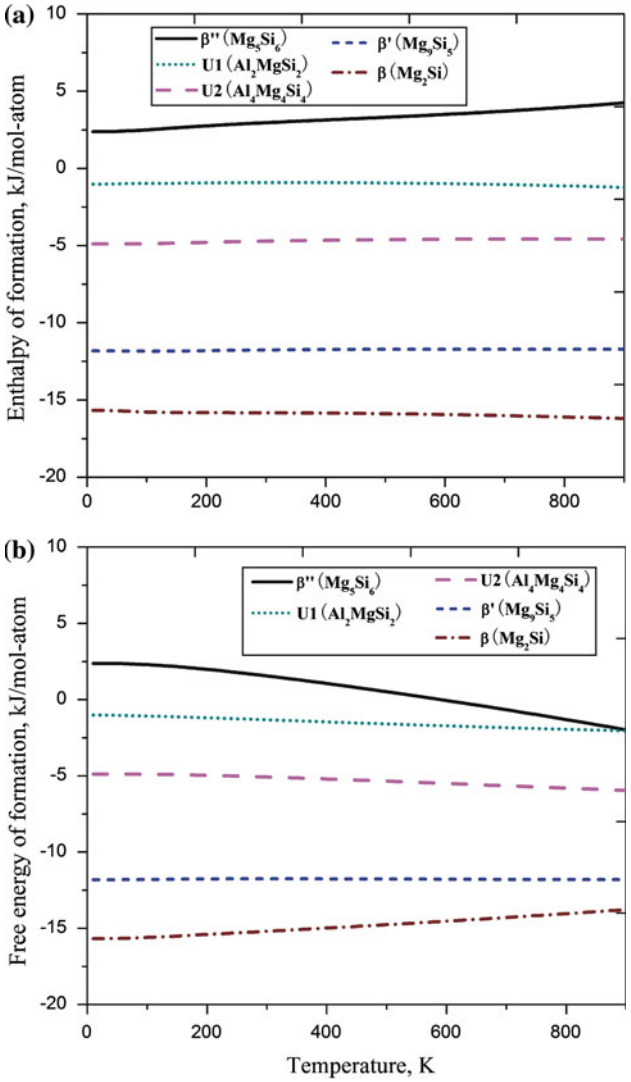

Fig. 11 Calculated formation enthalpies (**a**) and Gibbs formation energy (**b**) versus temperature based on quasiharmonic approach for the key precipitates β''-Mg_5Si_6, U1-Al_2MgSi_2, U2-$Al_4Mg_4Si_4$, β'-Mg_9Si_5, and β-Mg_2Si of the Al–Mg–Si alloys

Summary

A systematic investigation concerned with the structure, stability, and finite-temperature thermodynamic properties of the key precipitates in the Al–Mg–Si alloys including β''-Mg_5Si_6, U1-Al_2MgSi_2, U2-$Al_4Mg_4Si_4$, β'-Mg_9Si_5, and β-Mg_2Si have been conducted via first-principles calculations. The vibrational stability of these precipitated phases have been validated by the predicted phonon DOS's. The phonon LO/TO splitting of β-Mg_2Si has been accurately predicted with the mixed-space approach. The finite-temperature thermodynamic properties of these precipitated phases including entropy, enthalpy, and Gibbs free energy of these precipitates have been calculated based on the framework of the quasiharmonic approximation. In

particular, the heat capacities at constant pressure for these precipitates have been predicted. The finite-temperature entropies of formation, enthalpies of formation, and Gibbs free energy of formation of these precipitates have also been computed. The acquired thermodynamic properties of these precipitates are expected to be utilized for evaluating metastable equilibria in the Al–Mg–Si alloys.

Acknowledgement The financial supports from the National Natural Science Foundation of China (NSFC) (Grant Nos. 50831007, 50801069), State Key Laboratory of High Performance Ceramics and Superfine Microstructures, Shanghai Institute of Ceramics, Chinese Academy of Sciences (Grant No. SKL201102SIC) and National Basic Research Program of China (2011CB610401), are acknowledged.

References

1. Matsuda K, Ikeno S, Sato T, Kamio A (1996) Scr Mater 34:1797
2. Zandbergen HW, Andersen SJ, Jansen J (1997) Science 277:1221
3. Matsuda K, Gamada H, Fujll K, Uetani Y, Sato T, Kamio A, Ikeno S (1998) Metall Mater Trans A 29:1161
4. Matsuda K, Sakaguchi Y, Miyata Y, Uetani Y, Sato T, Kamio A, Ikeno S (2000) J Mater Sci 35:179. doi:10.1023/A:1004769305736
5. Ravi C, Wolverton C (2004) Acta Mater 52:4213
6. Andersen SJ, Marioara CD, Frøseth A, Vissers R, Zandbergen HW (2005) Mater Sci Eng A 390:127
7. Andersen SJ, Marioara CD, Vissers R, Frøseth A, Zandbergen HW (2007) Mater Sci Eng A 444:157
8. Frøseth AG, Høier R, Derlet PM, Andersen SJ, Marioara CD (2003) Phys Rev B 67:224106
9. Van Huis MA, Chen JH, Zandbergen HW, Sluiter MHF (2006) Acta Mater 54:2945
10. Van Huis MA, Chen JH, Sluiter MHF, Zandbergen HW (2007) Acta Mater 55:2183
11. Vissers R, Van Huis MA, Jansen J, Zandbergen HW, Marioara CD, Andersen SJ (2007) Acta Mater 55:3815
12. Liu F, Guo F, Chen H, Ouyang Y, Tao X, Feng Y, Du Y (2010) Z Metallkd 101:1392
13. Liu ZK (2009) J Phase Equil Diffus 30:517
14. Zhang H, Wang Y, Shang SL, Ravi C, Wolverton C, Chen LQ, Liu ZK (2010) CALPHAD 34:20
15. Fultz B (2009) Prog Mater Sci 55:247
16. Wang Y, Liu ZK, Chen LQ (2004) Acta Mater 52:2665
17. Arroyave R, Shin D, Liu ZK (2005) Acta Mater 53:1809
18. Shang SL, Wang Y, Kim D, Liu ZK (2009) Comput Mater Sci 47:1040
19. Mei ZG, Shang SL, Wang Y, Liu ZK (2009) Phys Rev B 80:104116
20. Zhang H, Shang SL, Wang Y, Saengdeejing A, Chen LQ, Liu ZK (2010) Acta Mater 58:4012
21. Kresse G, Furthmüller J (1996) Comput Mater Sci 6:15
22. Kresse G, Furthmüller J (1996) Phys Rev B 54:11169
23. Blöchl PE (1994) Phys Rev B 50:17953
24. Kresse G, Joubert D (1999) Phys Rev B 59:1758
25. Perdew JP, Burke K, Ernzerhof M (1996) Phys Rev Lett 77:3865
26. Monkhorst HJ, Pack JD (1976) Phys Rev B 13:5188
27. Blöchl PE, Jepsen O, Andersen OK (1994) Phys Rev B 49:16223
28. Van de Walle A (2009) CALPHAD 33:266
29. Sluiter MHF, Weinert M, Kawazoe Y (1999) Phys Rev B 59:4100
30. Wang Y, Wang JJ, Wang WY, Mei ZG, Shang SL, Chen LQ, Liu ZK (2010) J Phys Condens Matter 22:202201
31. Gajdoš M, Hummer K, Kresse G, Furthmüller J, Bechstedt F (2006) Phys Rev B 73:045112
32. Dinsdale AT (1991) CALPHAD 4:317
33. Straumanis ME (1949) J Appl Phys 20:726
34. Cooper AS (1962) Acta Crystallogr 15:578
35. Dutta BN (1962) Phys Status Solidi 2:984
36. Yu R, Zhu J, Ye HQ (2010) Comput Phys Commun 181:671
37. Bercegeay C, Bernard S (2005) Phys Rev B 72:214101
38. Nath K, Anderson AB (1988) Solid State Commun 66:277
39. Ganeshan S, Shang SL, Wang Y, Liu ZK (2009) Acta Mater 57:3876
40. Soma T (1981) Phys Status Solidi (b) 104:293
41. Shang SL, Saengdeejing A, Mei ZG, Kim DE, Zhang H, Ganeshan S, Wang Y, Liu ZK (2010) Comput Mater Sci 48:813
42. Tani J, Kido H (2008) Comput Mater Sci 42:531
43. Wang H, Jin H, Chu W, Guo Y (2010) J Alloys Compd 499:68
44. Mcwilliams D, Lynch DW (1963) Phys Rev 130:2248
45. Buchenauer CJ, Cardona M (1971) Phys Rev 3:2504
46. Baroni S, Gironcoli S, Corso AD, Giannozzi P (2001) Rev Mod Phys 73:515
47. Gerstein BC, Jelinek FJ, Habenschuss M, Shickell WD, Mullaly JR, Chung PL (1967) J Chem Phys 47:2109
48. Yuan X, Sun W, Du Y, Zhao D, Yang H (2009) CALPHAD 33:673
49. Kubaschewski O, Villa H (1949) Z Electrochem 53:32
50. Grjotheim K, Herstad O, Petrucci S, Skarbo R, Toguri J (1962) Rev Roum Chim 7:217
51. Ryabchikov IV, Mikulinski AS (1963) Izv Vyssh Uchebn Zaved Tsvet Met 1:95
52. Lukashenko GM, Eremenko VN (1964) Russ J Inorg Chem 9:1243
53. Mannchen W, Jacobo G (1965) Z Naturforsch 206:178
54. Caulfield HJ, Hudson DE (1966) Solid State Commun 4:299
55. Blachnik R, Kunze D, Schneider A (1971) Metall (Isernhagen, Germany) 25:119
56. Rao YK, Belton GR, Gokcen NA (ed) (1981) Chemical metallurgy: a tribute to carl wagner. The Metallurgical Society of AIME, New York
57. Owen EA, Preston GD (1924) Nature (Lond) 113:914
58. Feufel H, Godecke T, Lukas HL, Sommer F (1997) J Alloys Compd 247:31